DELPHI Collaboration DELPHI 2001-025 CONF 466
14 March, 2001

Searches for invisibly decaying Higgs bosons

André Sopczak, Marcel Stanitzki
Institut für experimentelle Kernphysik, Universität Karlsruhe
Guillelmo Gomez-Ceballos, Francisco Matorras
Instituto de Física de Cantabria, Universidad de Cantabria-CSIC

Abstract

Searches for HZ production with the Higgs boson decaying into an invisible final state have been updated with the latest data collected by the DELPHI experiment. Both hadronic and leptonic final states of the Z boson were analysed. No signal was found; good overall agreement with the Standard Model expectation was obtained. The results were also combined with those obtained in the searches for visible Higgs boson decay modes. The mass limit for invisibly decaying Higgs bosons is 113.0 GeV/c^2.

Contributed Paper for Moriond 2001

1 Introduction

This paper presents a search for the production of $e^+e^- \rightarrow HZ$ with $Z \rightarrow q\bar{q}$ or $Z \rightarrow \ell^+\ell^-$ and the Higgs decaying into stable non-interacting particles rendering it invisible (Fig. 1). Such invisible Higgs decays can occur in Supersymmetry [1] or other models like Majoron models [2, 3, 4]. The search described here was performed on the data collected by DELPHI in the high energy runs at 189 to 209 GeV centre-of-mass energy.

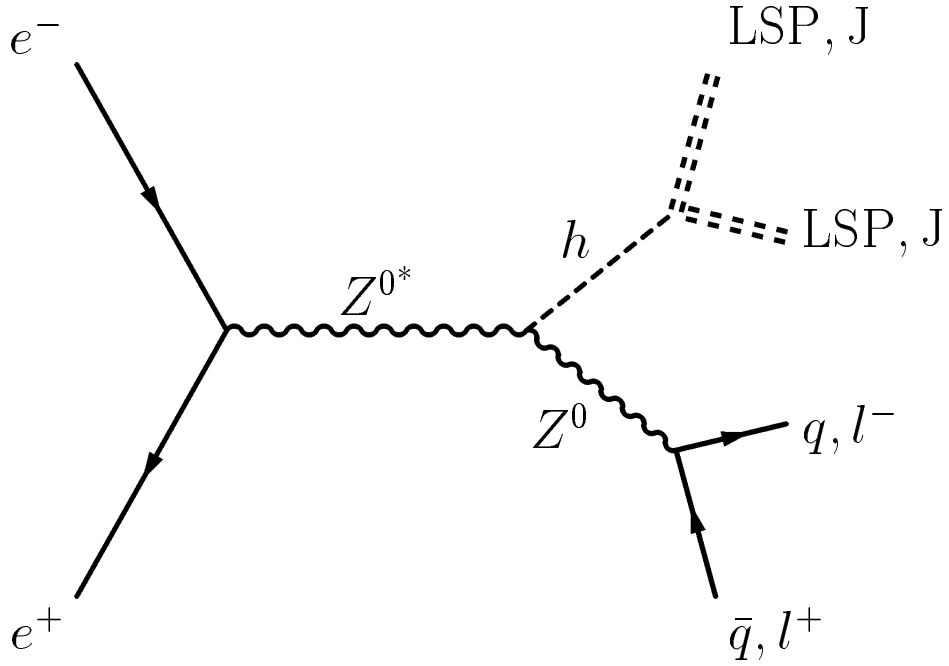

Figure 1: Feynman graph describing the HZ production with the Higgs decaying into invisible particles, e.g. the lightest supersymmetric particle (LSP) or a Majoron (J) in models with an extended Higgs sector.

2 The DELPHI Detector

The general criteria for the selection of the events are mainly based on the information from the tracking system, the calorimeters and the muon chambers of the DELPHI detector. The DELPHI detector and its performance are described in detail in Ref. [5]. The vertex detector was upgraded in recent years [6], and a set of scintillation counters were added to veto photons in blind regions of the electromagnetic calorimeter at polar angles near 40 and 90 degree. One of the TPC sectors (S6) was not operational during the last period of the high energy data taking in 2000 . These data were analysed separately and then combined with the results from the previous periods. The performance of the analyses were found to be compatible within statistical errors.

3 The hadronic channel

The hadronic decay of the Z represents 70% of the HZ final states. The signature of an invisible Higgs boson decay is a pair of acoplanar and acollinear jets with a mass compatible with the Z mass and the missing energy and momentum of the invisibly decaying boson. The analysed data sample corresponds to an integrated luminosity of about 592 pb^{-1} at centre-of-mass energies from 189 to 209 GeV.

The background processes $\mathrm{e^+e^-}\to\mathrm{q\bar{q}}(n\gamma)$ were generated using the Monte Carlo generator `PYTHIA` [8]. Processes leading to charged and neutral current four-fermion final states were generated with the `EXCALIBUR` generator [9]. In the final state $\mathrm{q\bar{q}}e\bar{\nu}$, the `GRC4F` generator [10], with fermion mass effects included, was used to describe the phase space at low electron polar angles, where the finite electron mass is relevant. The `GRC4F` generator was also used in the Ze^+e^- dominated final states, where either one or both electrons escape undetected below 11.5°. The `TWOGAM` program [11] was used to describe the two-photon interactions. For the signal simulation the `HZHA` generator [12] was used. For the different years the following different samples were used:

- **1998:** 60 to 90 GeV/c^2 in 5 GeV/c^2 and 90 to 105 GeV/c^2 in 2.5 GeV/c^2 steps.
- **1999:** 85 to 100 GeV/c^2 in 5 GeV/c^2 and 100 to 107.5 GeV/c^2 in 2.5 GeV/c^2 steps.
- **2000:** 90 to 100 GeV/c^2 in 5 GeV/c^2 and 100 to 115.0 GeV/c^2 in 2.5 GeV/c^2 steps.

Both signal and background events were processed through the full DELPHI detector simulation [5].

3.1 Preselection

The preselection consisted of four steps.

3.1.1 Detector quality veto

A detector quality selection was used, requiring that both the tracking system and the calorimeters be fully operational.

3.1.2 Anti-$\gamma\gamma$

This selection suppresses most of the $\gamma\gamma$ background. Each event was required to have at least 9 charged tracks, 2 tracks with a good impact parameter, the charged energy greater than $0.16\sqrt{s}$, no electromagnetic shower with more than $0.45\sqrt{s}$, the transverse energy greater than $0.15\sqrt{s}$ and the sum of the longitudinal momenta greater than $0.25\sqrt{s}$.

3.1.3 Anti-radiative return

This selection was applied to suppress most of the background events resulting from radiative return to the Z-pole. It contained a two-dimensional cut in the $\theta_{\mathrm{p_{mis}}}$ vs. E′ plane, requiring

$\theta_{\mathrm{p_{mis}}} \geq 40^\circ$ and $\mathrm{E}' \geq 115$ GeV,

$\theta_{\mathrm{p_{mis}}} \leq 140^\circ$ and $\mathrm{E}' \geq 115$ GeV,

where E′ stands for the effective centre-of-mass energy after the emission of the first photon and $\theta_{\mathrm{p_{mis}}}$ is polar angle of the missing momentum. Furthermore, less than $0.08\sqrt{s}$ had to be deposited in the STIC[1] [5], $\mathrm{E}'/\sqrt{\mathrm{s}}$ had to be less $0.96\sqrt{s}$ and the total electromagnetic energy below 30° had to be less than $0.16\sqrt{s}$. In order to suppress badly reconstructed events, candidates in which jets pointed to cracks between barrel and endcap detectors, or where both jets were below 12° were rejected. A hermeticity veto algorithm was applied to ensure that no photon had escaped in the blind region of the electromagnetic calorimeter at polar angles near 40 and 90 degrees. The energy of the leading particle or electromagnetic shower was required to be less than $0.2\sqrt{s}$ and the transverse momentum with respect to the jet (forcing the event into a two-jet configuration) to be less than 0.05. Finally, we required that upon forcing the event into a three-jet configuration, every jet have at least one charged track.

3.1.4 Tail cuts and IDA step

Twelve variables were used to construct a performant tagging variable in the framework of an Iterative Discriminant Analysis Program (IDA) [13]. In order to calculate these variables, the event was forced into 2 jets, using the DURHAM [14] algorithm.

- $E_\gamma/E_\gamma^{\mathrm{Z}}$: the normalised energy of a photon assumed to have escaped in the beam direction, deduced from the polar angles of the two main jet directions in the event. The photon energy estimate was normalised to the energy expected for a photon recoiling against an on-shell Z.
- $\ln(p_{\mathrm{T(Event)}})$: the logarithm of the transverse momentum of the event.
- $E_{\mathrm{vis}}/\sqrt{s}$: the visible energy of the event, normalised by the centre-of-mass energy;
- $E_{\mathrm{T}}/\sqrt{s}$: the transverse energy of the event, normalised by the centre-of-mass energy;
- $E(\theta < 20^\circ)/\sqrt{s}$: The energy below 20°, normalized by the centre-of-mass energy;
- $\cos(\vec{p}_{\mathrm{mis}})$: the cosine of the missing momentum angle to the z-axis;
- $E_{\mathrm{isol}}/\sqrt{s}$: the energy sum in the double cone, defined by half opening angles 5 and α_{max} around the most isolated particle, divided by its energy. The most isolated particle is defined as the particle with momentum above 2 GeV/c with the smallest energy sum in the double cone. In the momentum interval from 2 to 5 GeV/c, α_{max} is set to 60° in order to maximise the sensitivity to isolated particles from tau decays in $\mathrm{WW} \to \mathrm{q\bar{q}}'\tau\nu$ events, while an opening angle of 25° is used for particles with higher momenta;
- $p_{\mathrm{isol}}/\sqrt{s}$: the momentum of the most isolated particle, as defined above;
- Scaled Acoplanarity: the log_{10} of the scaled acoplanarity. Acoplanarity is defined as 180°-$\Delta\phi$, where $\Delta\phi$ is the difference in azimuthal angle between the two jets, when forcing the reconstruction in exactly two jets. In order to compensate for the

[1] Small angle TIle Calorimeter, covering the very forward region

Variable	lower cut	upper cut
E_γ/E_γ^Z	0.0	0.90
$\ln(p_{\mathrm{T(Event)}})$	1.75	4.5
$E_{\mathrm{vis}}/\sqrt{s}$	-	-
$E_{\mathrm{T}}/\sqrt{s}$	0.15	0.6
$E(\theta < 20^\circ)/\sqrt{s}$	-	-
$\cos(\vec{p}_{\mathrm{mis}})$	0.0	1.0
$E_{\mathrm{isol}}/\sqrt{s}$	-	-
$p_{\mathrm{isol}}/\sqrt{s}$	0.008	0.18
Scaled Acoplanarity	0.3	2.5
Thrust	0.65	1.0
ln(Acollinearity)	2.0	4.5
$\ln(\max(\mathrm{p_T})_{\mathrm{Jet}})$	-0.5	2.50

Table 1: The tail cuts used in the analysis, the variables are described in detail in [7]

geometrical instability of this variable for jets at low angles it was scaled with the angle between the 2 jets;

- Thrust: the thrust, computed in the rest frame of the visible system. The transformation into the rest frame is made in order to compensate the smearing due to the boost of the jet system;
- ln(Acollinearity): the logarithm of the acollinearity of the two-jet system.
- $\ln(\max(\mathrm{p_T})_{\mathrm{Jet}})$: the largest transverse momentum of the jet-particles, defined by the transverse momentum of any particle with respect to the nearest jet.

Cuts were applied in the tails of these variable distributions in order to concentrate on the signal region in the optimization (Tab. 1).

In addition, the signal was further enriched by requiring that the number of identified leptons in an event be less than three.

Two IDA steps were performed in order to obtain optimal signal to background discrimination. The background versus efficiency curve is shown in Fig. 2. The working point determined by maximising the expected mass limit as a function of efficiency, is indicated by the dashed line in Fig. 2. This working point was obtained separately for each centre-of-mass energy, optimizing the analysis for a 85 GeV/c^2 Higgs at 189 GeV, for a 95 GeV/c^2 Higgs at 192 and 196 GeV, for a 100 GeV/c^2 Higgs at 200 and 202 GeV and for a 105 GeV/c^2 Higgs for 2000 data.

3.2 Mass reconstruction

The recoil mass to the di-jet system, which corresponds to the mass of the invisible Higgs, was calculated taking into account a Z-mass constraint for the measured di-jet system, from the visible energy and the visible mass, using the following expression

$$m_{\mathrm{inv}} = \sqrt{\left(\sqrt{\mathrm{s}} - \frac{m_{\mathrm{Z}} E_{\mathrm{vis}}}{m_{\mathrm{vis}}}\right)^2 - \left(\frac{m_{\mathrm{Z}} p_{\mathrm{mis}}}{m_{\mathrm{vis}}}\right)^2},$$

where p_{mis} is the missing momentum and m_{Z} is the Z mass. The recoil mass distribution after the final selection is shown in Fig. 3.

3.3 Systematic errors

Only a partial study of systematic errors has been done in the context of these preliminary results. The effect of the modeling of the QCD fragmentation in the $\mathrm{q\bar{q}}(n\gamma)$ background was studied by replacing the PYTHIA generator with the ARIADNE generator [15] at 189 GeV. The result was 12.41 $\pm$1.00 events (ARIADNE) compared to 11.51 $\pm$ 0.55 (PYTHIA) events. This result is compatible within the statistical error. The error of the luminosity and the signal cross section is assumed to be 1 %. Uncertainties on the cross-sections of the SM background processes were not considered yet. The total systematic error, combined with the MC statistics is shown in Tab. 2.

4 Leptonic channels

The $\mathrm{H}\ell^+\ell^-$ represents about 10% of the HZ final state. The experimental signature of the HZ($\mathrm{Z} \to \ell^+\ell^-$) final states is a pair of acoplanar and acollinear leptons, with an invariant mass compatible with the expectation from $\mathrm{Z} \to \ell^+\ell^-$ in the case of muons and electrons. The signal and the background simulations were performed with the same programs as the hadronic channel, except that the KORALZ generator [16] was used to describe the $\mu^+\mu^-(\mathrm{n}\gamma)$ and $\tau^+\tau^-(\mathrm{n}\gamma)$ background and the BHWIDE generator [17] was used for the Bhabha processes. The leptonic two-photon processes were generated with BDK [18]. The relevant backgrounds arise from W-pairs, di-leptons from $\mathrm{e^+e^-} \to \mathrm{Z}(\gamma)$, Bhabha scattering, two-photon collisions, $\mathrm{Ze^+e^-}$, ZZ and $\mathrm{l}\nu\mathrm{e}\nu$ processes.

4.1 Leptonic preselection

An initial set of cuts was applied to select a sample enriched in leptonic events. All particles in an event were clustered into jets using the LUCLUS algorithm [19] (d_{join} = 6.5 GeV/c) and only events with two reconstructed jets, containing at least one charged particle each, were retained. A charged particle multiplicity between 2 and 5 was required and at least one jet had to consist of only one charged particle. In order to reduce the background from two-photon collisions and radiative di-lepton events, both the event acoplanarity, θ_{acop}, and the acollinearity of the two jet directions projected onto the plane perpendicular to the beam axis, had to be larger than 2 degrees. In addition, the total momentum transverse to the beam direction, P_t, had to exceed $0.02\sqrt{s}$. To reduce the W-pair contribution the acollinearity of the two jet directions had to be between 3 and 60 degrees as shown in Fig. 4. Finally, the energy of the most energetic photon was required to be less than $0.15\sqrt{s}$, and the angle between that photon and the charged system projected onto the plane perpendicular to the beam axis had to be less than 170 degrees.

4.2 Channel Identification

For this sample jets were then identified as either μ, e or τ and two leptons with the same flavour were required. A particle was identified as a muon if at least one hit in

the muon chambers was associated to it, or if it had energy deposited in the outermost layer of the hadron calorimeter; in addition the energy deposited in the other layers had to be compatible with that from a minimum ionizing particle. For the identification of a particle as an electron the energies deposited in the electromagnetic calorimeters, in the different layers of the hadron calorimeter, and in addition the energy loss in the time projection chamber were used. A lepton was identified as a cascade decay coming from a τ if the momentum was lower than $0.13\sqrt{s}$.

4.3 Channel dependent criteria

After the preselection, if both jets were identified as either muons, electrons or taus, different cuts were applied in each channel in order to reduce the remaining background.

In the $\mu^+\mu^-$ channel the direction of the missing momentum had to deviate from the beam axis by more that 18° in order to reject $\mu^+\mu^-(\gamma)$ and $\gamma\gamma \to \mu^+\mu^-$ processes. The momentum of the most energetic muon had to be between $0.2\sqrt{s}$ and $0.4\sqrt{s}$ and the visible energy less than $0.55\sqrt{s}$. Finally, the di-muon mass was required to be between 75 GeV/c^2 and 97.5 GeV/c^2, to be consistent with the Z boson mass.

In the e^+e^- channel, the most important background arises from radiative Bhabha scattering and Ze^+e^- events. To suppress these backgrounds, the direction of the missing momentum and the polar angle of both leptons had to deviate from the beam axis by more that 18°. In addition, the total associated energy was required to be less than $0.55\sqrt{s}$, the energy for both leptons less than $0.35\sqrt{s}$ and the neutral electromagnetic energy less than $0.1\sqrt{s}$. Finally, the invariant mass of both leptons has to be between 75 GeV/c^2 and 100 GeV/c^2, to be consistent with the Z boson mass.

In the $\tau^+\tau^-$ channel tighter cuts were applied on the acoplanarity and acollinearity in order to reduce remaining background from $\tau^+\tau^-(\gamma)$ and $\gamma\gamma \to \ell\ell$ processes. The invariant mass of both jets had to be less than 3 GeV/c^2. In addition the transverse energy had to be greater than $0.1\sqrt{s}$ and the visible energy of all particles with $|\cos\theta| < 0.9$ had to be greater than $0.06\sqrt{s}$. Finally, the energy of both jets had to be less than $0.26\sqrt{s}$.

4.4 Systematic uncertainties

Different systematic checks were performed on the leptonic selection. First, all variables were checked at preselection level and after all cuts except that on the studied variable. In all cases there was agreement within statistical errors.

The effect of the different 4-fermions generators was studied by comparing PYTHIA and EXCALIBUR samples. Good agreement was observed. The only significant discrepancy of the data with both generators was on the rate of emitted radiative photons. We estimated the impact of this disagreement on the final selection by extrapolating the energy spectra obtained before applying the cuts to the cut region. This yielded a relative uncertainty of about 1% on the detection efficiency.

The particle identification was checked using leptonic Z decays to be well described at the 1% level. The effect on the expected background was therefore estimated to be 2%. Similarly the track reconstruction efficiency was checked on the same samples and on $\gamma\gamma$ samples, especially in the detector boundaries. This contribution amounted to 0.6%. The total systematic error, combined with the MC statistics is shown in Tab. 2.

4.5 Mass reconstruction

The mass of the invisibly decaying particle was computed from the measured energies assuming momentum and energy conservation. To improve the resolution a χ^2 fit was applied constraining the visible mass to be compatible with a Z. In the case of the $\tau^+\tau^-$ channel, the information carried by the decay products does not reproduce correctly the τ energy. Therefore, we calculated the mass under the assumption that both τ leptons had the same energy. This, together with the visible mass constraint, allowed an estimation of this energy and of the invisible mass. The invisible mass for the candidates as well as for the expected background from Standard Model processes for the different channels is shown in Fig. 5.

5 Results

The results of the analysis of the four channels are summarized in Tab. 2, in the form of a comparison of observed and predicted selected events. The agreement between data and background is good for all channels and no indication of an invisible Higgs boson signal is observed.

6 Limits

6.1 Model independent limits

The cross-section and mass limits were computed again with a likelihood method [20]. All search channels and center-of-mass energies are treated as separate experiments to obtain a likelihood function.

Figure 6 displays the observed and expected upper limits on the cross-section for the process $e^+e^- \to Z(\text{anything})H(\text{invisible})$ as a function of the Higgs mass. From the comparison with the Standard Model Higgs cross-section the observed (expected median) mass limits are 113.0 (110.7) GeV/c^2.

In general, the branching ratio into invisible particles BR_{inv} is a free parameter. The remaining decay modes are then visible and are assumed to follow the SM decay probabilities. In this case the searches for visible and invisible Higgs decays can be combined to determine the excluded region in the BR versus m_H plane assuming SM production cross-sections. Using the DELPHI limits on the visible cross-section [21] a lower mass limit of 112.7 GeV/c^2 can be set independent of the hypothesis on the fraction of invisible decay modes, as shown in Fig. 7. In computing these limits, the overlap between the standard $H\nu\bar{\nu}$ and the invisible Higgs hadronic selections have been avoided, conservatively for the limit, by omitting the $H\nu\bar{\nu}$ ($H_{\text{inv}}q\bar{q}$) results in the region $BR_{\text{inv}} > 50\%(< 50\%)$.

6.2 Limits for a Majoron Model

The limits computed above can be used to set a limit on the Higgs bosons in a Majoron model with one doublet ϕ and one singlet η. Mixing of the real parts of ϕ and η leads to two massive Higgs bosons:

$$H = \phi_R \cos\theta - \eta_R \sin\theta$$

$$S = \phi_R \sin\theta + \eta_R \cos\theta$$

where θ is the mixing angle. The imaginary part of the singlet is identified as the Majoron. The Majoron is decoupled from the fermions and gauge bosons, but might have a large coupling to the Higgs bosons. In this model the free parameters are the masses of H and S, the mixing angle θ and the ratio of the vacuum expectation values of the two fields ϕ and η ($\tan\beta \equiv \frac{v_\phi}{v_\eta}$). The production rates of the H and S are reduced with respect to the SM Higgs boson, by factors of $\cos^2\theta$ and $\sin^2\theta$, respectively. The decay widths of the H and S into the heaviest possible fermion-antifermion pair are reduced by the same factor and their decay widths into a Majoron pair are proportional to the complementary factors ($\cos^2\theta$ for S and $\sin^2\theta$ for H). Concentrating on the case where the invisible Higgs decay mode is dominant ($\tan\beta$ large), the excluded region in the mixing angle versus Higgs mass plane is shown in Fig. 8.

7 Conclusion

In data samples of about 590 pb^{-1} collected by the DELPHI detector at a centre-of-mass energy of 189 to 209 GeV, 140 hadronic, 12 muon pair, 15 electron pair and 25 tau pair events were selected in searches for a Higgs boson decaying into invisible modes. These numbers are consistent with the expectation from SM background processes.

We set a 95% CL lower mass limit of 113.0 GeV/c^2 for Higgs bosons with a Standard Model cross-section and with 100% branching fraction into invisible decays. By combining this search for invisible decays with previous limits on visible decays we set a 95% CL lower mass limit of 112.7 GeV/c^2 for a Higgs boson with an arbitrary invisible branching fraction.

References

[1] A. Djouadi, P. Janot, J. Kalinowski and P.M. Zerwas, *Phys. Lett.* **B376** (1996) 220

[2] Y. Chikashige, R.N. Mohapatra, R.D. Peccei, *Phys. Lett.* **B98** (1981) 265;
R.E. Shrock, M. Suzuki, *Phys. Lett.* **B110** (1982) 250;
R. Mohapatra, J.W.F. Valle, *Phys. Rev.* **D34** (1986) 1642;
M.C. Gonzalez-Garcia, J.W.F. Valle, *Phys. Lett.* **B216** (1989) 360;
E.D Carlson, L.J. Hall, *Phys. Rev.* **D40** (1989) 3187;
L.F. Li,Y. Liu, L. Wolfenstein, *Phys. Lett.* **BB159** (1985) 45;
A. Zee, *Phys. Lett.* **B93** (1980) 389.

[3] F. de Campos et al.,*Phys. Rev.* **D55** (1997) 1316.

[4] S.P. Martin and J.D. Wells, *Phys. Rev.* **D60** (1999) 035006

[5] DELPHI Collaboration, P. Abreu et al., *Nucl. Instr. and Meth.* **378** (1996) 57;
DELPHI Collaboration, P. Aarnio et al, *Nucl. Instr. and Meth.* **A303** (1991) 233

[6] DELPHI Silicon Tracker Group,P. Chochula et al., *Nucl. Instr. and Meth.* **A412** (1998) 304

[7] DELPHI Collaboration, P. Abreu et al., *Phys. Lett. B 459* (1999) 367.

[8] T. Sjöstrand, *Comp. Phys. Comm.* **39** (1986) 347; *Comp. Phys. Comm.* **82** (1994) 74.

[9] F.A. Berends, R. Pittau, R. Kleiss, *Comp. Phys. Comm.* **85** (1995) 437.

[10] Y. Kurihara et al., Vol. 2, p. 30 in *Physics at LEP2* G. Altarelli, T. Sjöstrand and F. Zwirner (eds.) CERN 96-01 (1996).

[11] S. Nova et al. in CERN Report 96-01, Vol. 2, p. 224.

[12] P. Janot, in CERN Report 96-01, Vol. 2, p. 309.

[13] T.G.M. Malmgren, *Comp. Phys. Comm.* **106** (1997) 230;
T.G.M. Malmgren and K.E. Johansson, *Nucl. Instr. and Meth.* **403** (1998) 481.

[14] S. Catani, Y. L. Dokshitzer, M. Olsson, G. Turnock and B. R. Webber, annihilation," Phys. Lett. **B269** (1991) 432.

[15] L. Lonnblad, implementing the color dipole model," Comput. Phys. Commun. **71** (1992) 15.

[16] S. Jadach, W. Placzek and B. F. Ward, *Phys. Lett.* **B390** (1997) 298

[17] S. Jadach, B. F. Ward and Z. Was, *Comp. Phys. Comm.* **79** (1994) 503.

[18] F.A. Berends, P.H. Daverveldt, R. Kleiss, *Nucl. Phys.* **B253** (1985) 421; Comput. Phys. Commun. **40** (1986) 271, 285 and 309.

[19] T. Sjöstrand, *PYTHIA 5.7 / JETSET 7.4*, CERN-TH.7112/93 (1993).

[20] A.L. Read, in CERN Report 2000-005 p. 81 (2000).

[21] DELPHI Collaboration, P. Abreu et al., contribution to the Moriond conference 2001, CERN-EP/2001-004, *Search for the Standard Model Higgs boson at LEP in the year 2000.*

$\sqrt{s}$ GeV	Channel	Lumin. pb^{-1}	Data	Expected Bkg.	Signal eff. %
189	$q\bar{q}$	152.8	47	51.5 $\pm$1.0	40.9$\pm$1.5
192	$q\bar{q}$	24.9	6	8.6 $\pm$0.6	46.0$\pm$1.6
196	$q\bar{q}$	75.0	32	29.5 $\pm$0.3	56.3$\pm$1.6
200	$q\bar{q}$	82.2	16	12.8 $\pm$0.5	44.0$\pm$1.6
202	$q\bar{q}$	40.4	9	8.0 $\pm$0.3	48.1$\pm$1.6
205	$q\bar{q}$	76.3	9	12.6 $\pm$0.3	40.2$\pm$1.1
206.7	$q\bar{q}$	82.8	10	13.3 $\pm$0.3	36.7$\pm$1.1
206.7S	$q\bar{q}$	58.0	11	10.2 $\pm$0.3	40.0$\pm$1.5
189	$\mu^+\mu^-$	153.81	4	3.68$\pm$0.3	62.2$\pm$1.5
192	$\mu^+\mu^-$	24.53	3	0.70$\pm$0.1	62.2$\pm$1.5
196	$\mu^+\mu^-$	72.44	1	2.03$\pm$0.2	62.2$\pm$1.5
200	$\mu^+\mu^-$	81.77	1	2.16$\pm$0.2	62.2$\pm$1.5
202	$\mu^+\mu^-$	39.44	1	1.09$\pm$0.2	61.4$\pm$1.5
205	$\mu^+\mu^-$	69.09	0	2.20$\pm$0.2	61.4$\pm$1.5
206.7	$\mu^+\mu^-$	79.83	2	1.98$\pm$0.2	61.3$\pm$1.5
206.7S	$\mu^+\mu^-$	50.04	0	1.36$\pm$0.2	58.4$\pm$1.6
189	e^+e^-	153.81	4	4.67$\pm$0.5	47.8$\pm$1.6
192	e^+e^-	24.53	0	0.93$\pm$0.2	47.8$\pm$1.6
196	e^+e^-	72.44	4	2.38$\pm$0.3	47.8$\pm$1.6
200	e^+e^-	81.77	3	2.88$\pm$0.4	47.8$\pm$1.6
202	e^+e^-	39.44	0	1.19$\pm$0.2	46.3$\pm$1.5
205	e^+e^-	66.09	2	2.15$\pm$0.2	44.9$\pm$1.6
206.7	e^+e^-	79.83	1	2.54$\pm$0.3	46.1$\pm$1.6
206.7S	e^+e^-	50.04	1	1.50$\pm$0.3	41.7$\pm$1.6
189	$\tau^+\tau^-$	153.81	7	7.13$\pm$0.7	18.9$\pm$1.4
192	$\tau^+\tau^-$	24.53	1	1.15$\pm$0.3	24.3$\pm$1.4
196	$\tau^+\tau^-$	72.44	5	3.40$\pm$0.4	24.3$\pm$1.4
200	$\tau^+\tau^-$	81.77	4	4.31$\pm$0.5	24.3$\pm$1.4
202	$\tau^+\tau^-$	39.44	1	2.25$\pm$0.3	26.2$\pm$1.4
205	$\tau^+\tau^-$	69.09	3	3.64$\pm$0.4	28.9$\pm$1.5
206.7	$\tau^+\tau^-$	79.83	2	4.09$\pm$0.5	27.5$\pm$1.5
206.7S	$\tau^+\tau^-$	50.04	0	2.86$\pm$0.4	26.9$\pm$1.5

Table 2: Integrated luminosity, observed number of events, expected number of background events and signal efficiency (100 GeV/c^2 signal mass) for different energies. The last lines in each section refers to the data taken with one TPC sector inoperative, which has been fully taken into account in the event simulations.

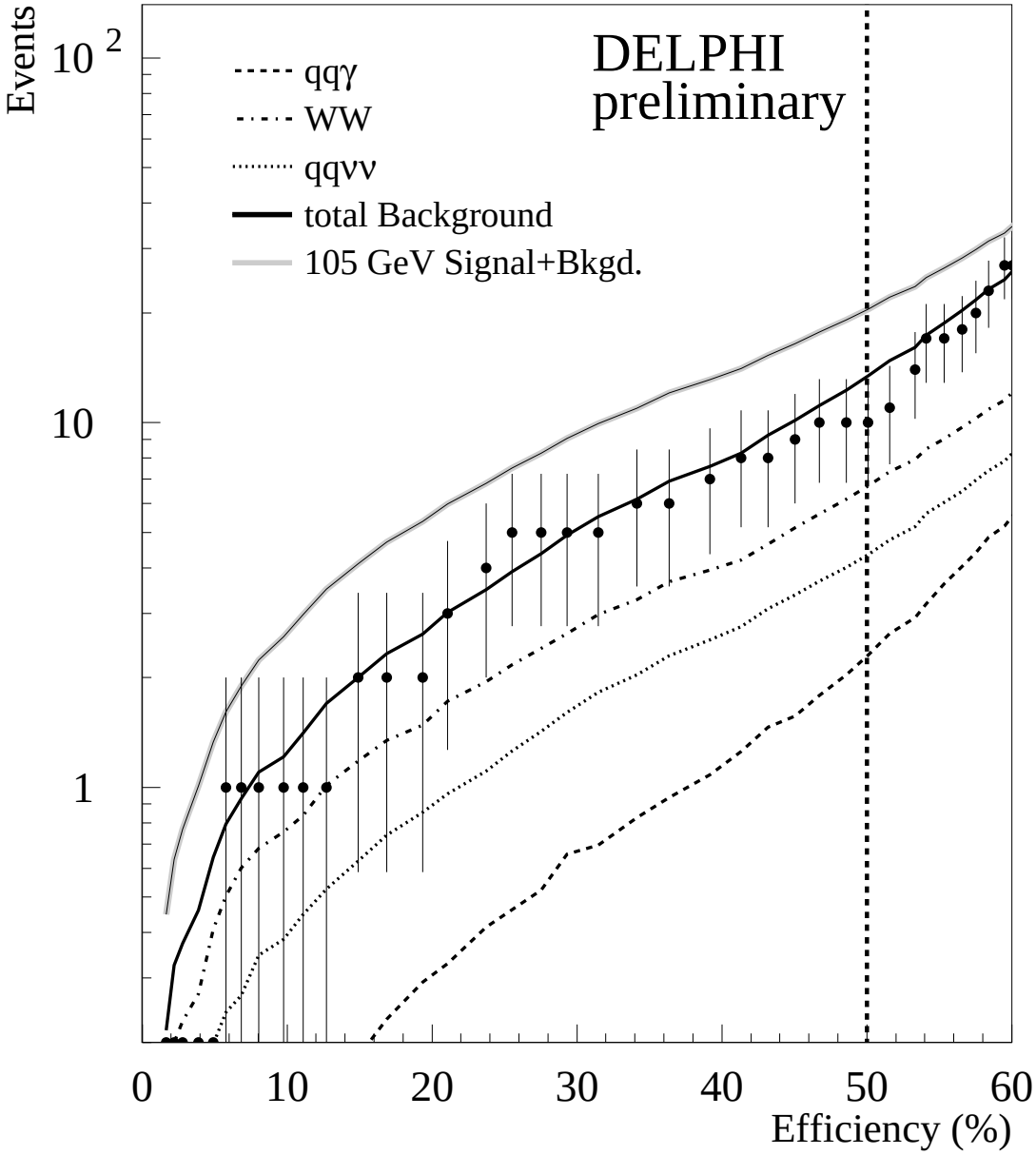

Figure 2: Expected background for the 206.7 GeV data as a function of the efficiency for a Higgs signal of 105 GeV/c^2 in the hadronic channel. The indicated lines represent the most important backgrounds with the solid black line showing the sum of all the background processes. In addition the grey line shows the expectation for a 105 GeV Higgs signal added on top of the background. The vertical dashed line indicates the working point chosen to optimize the sensitivity (see the text).

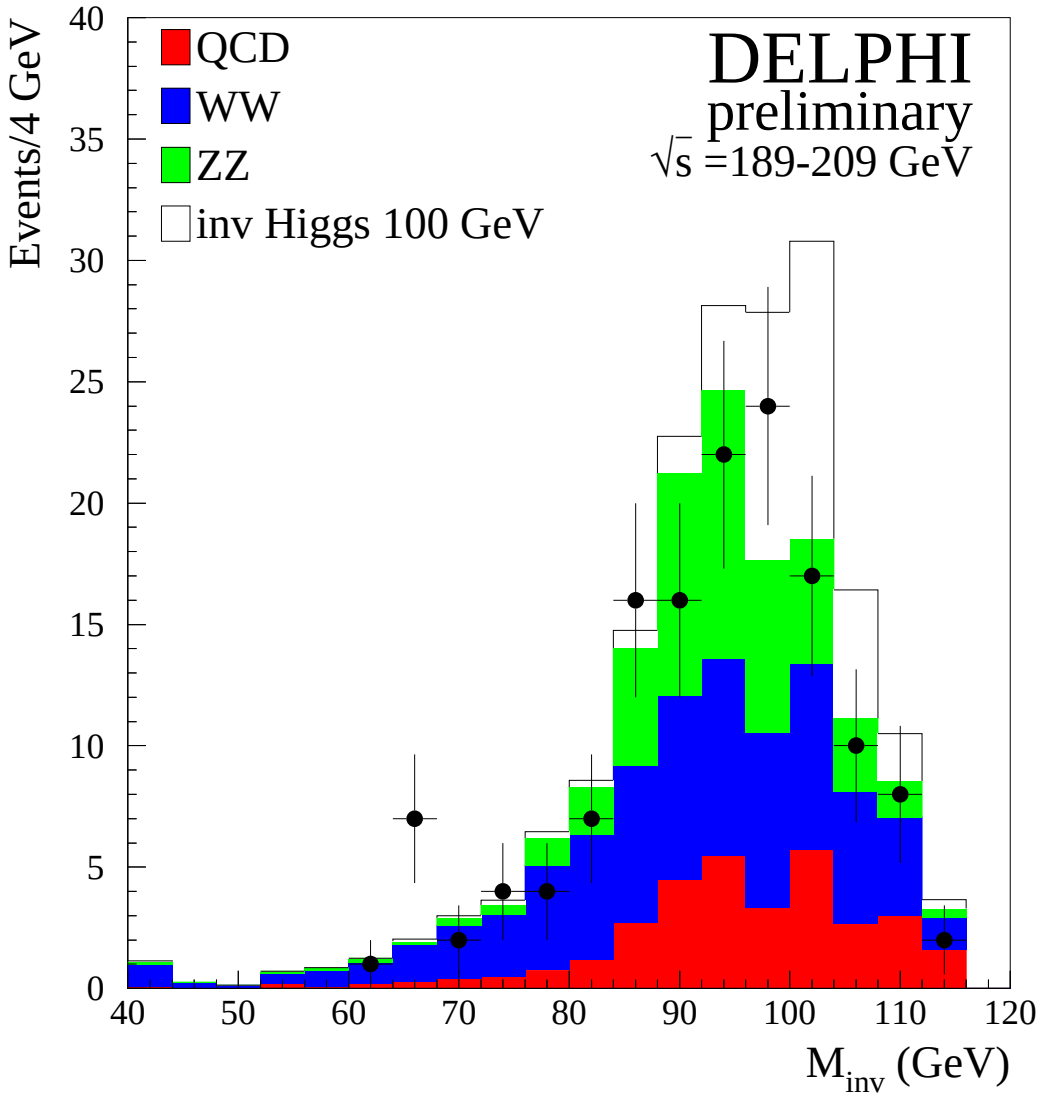

Figure 3: Reconstructed Higgs mass for all candidates in the Hq$\bar{q}$ channel for 189 to 209 GeV.

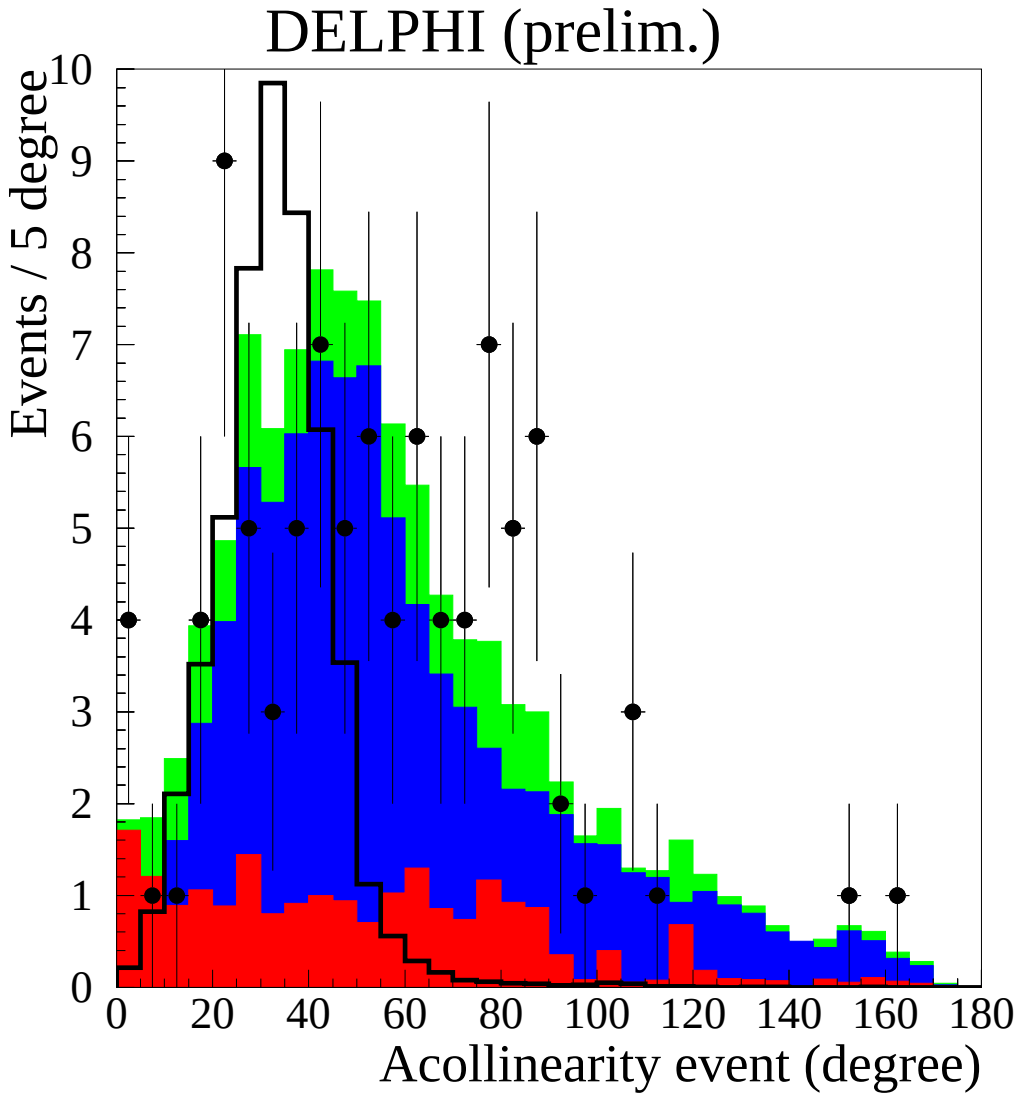

Figure 4: Acollinearity distribution in the h$\ell^+\ell^-$ channel for 189 to 209 GeV. The color codes describing the MC components are the same as in the previous figure.

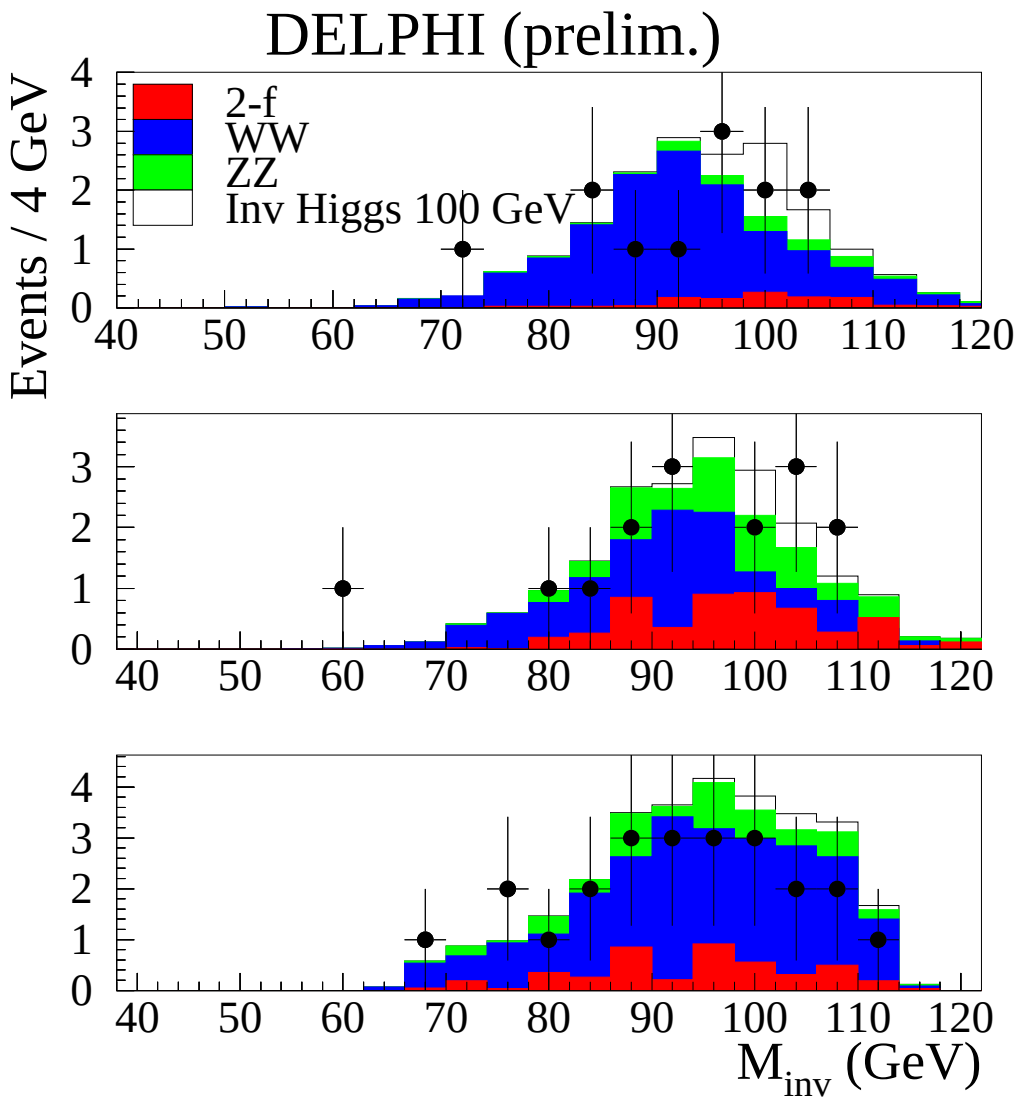

Figure 5: Reconstructed Higgs mass for all candidates in the h$\ell^+\ell^-$ channel for 189 to 209 GeV.

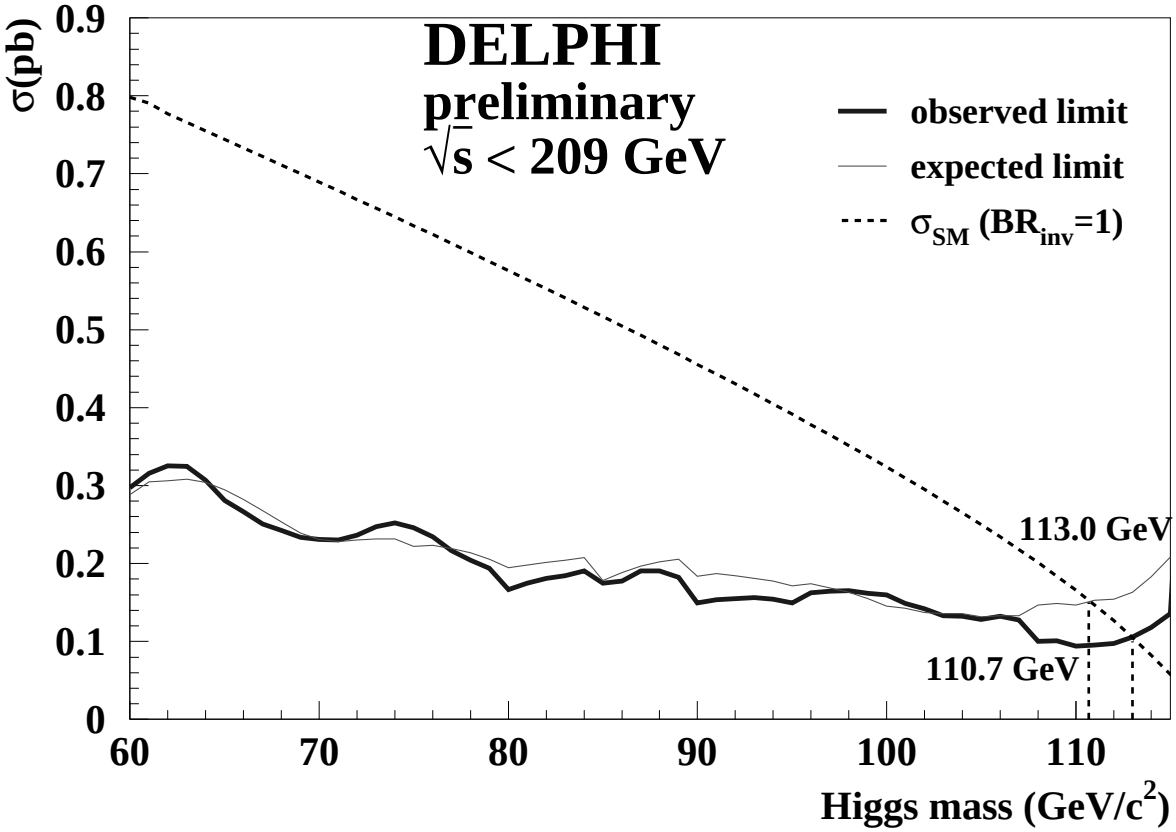

Figure 6: The 95% CL upper limit on the cross-section $e^+e^- \to Z(\text{anything})\, H(\text{invisible})$ as a function of the Higgs boson mass. The dashed line shows the standard model cross-section for the Higgs production with a BR_{inv} of 100%.

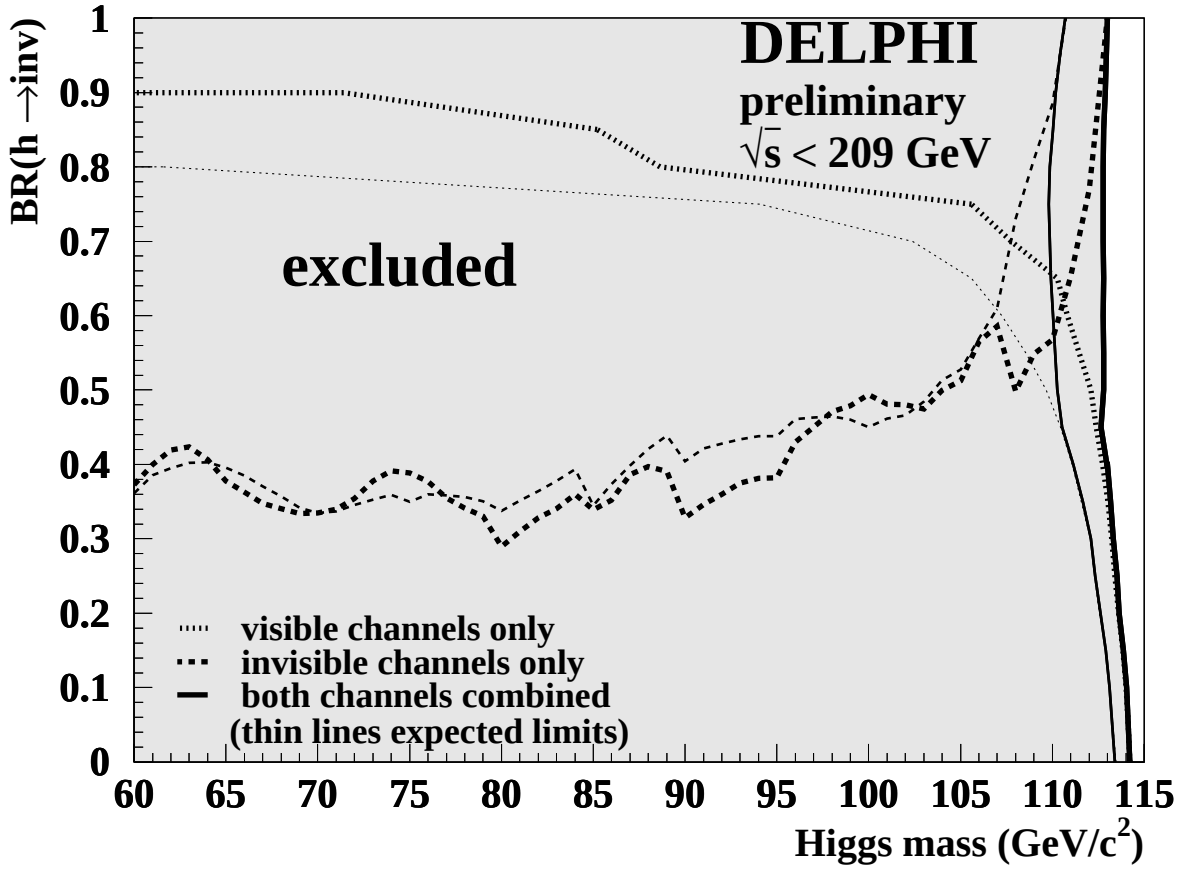

Figure 7: The excluded Higgs limits as function of the branching ratio into invisible decays BR_{inv}, assuming a $1 - BR_{inv}$ branching ratio into standard visible decay modes.

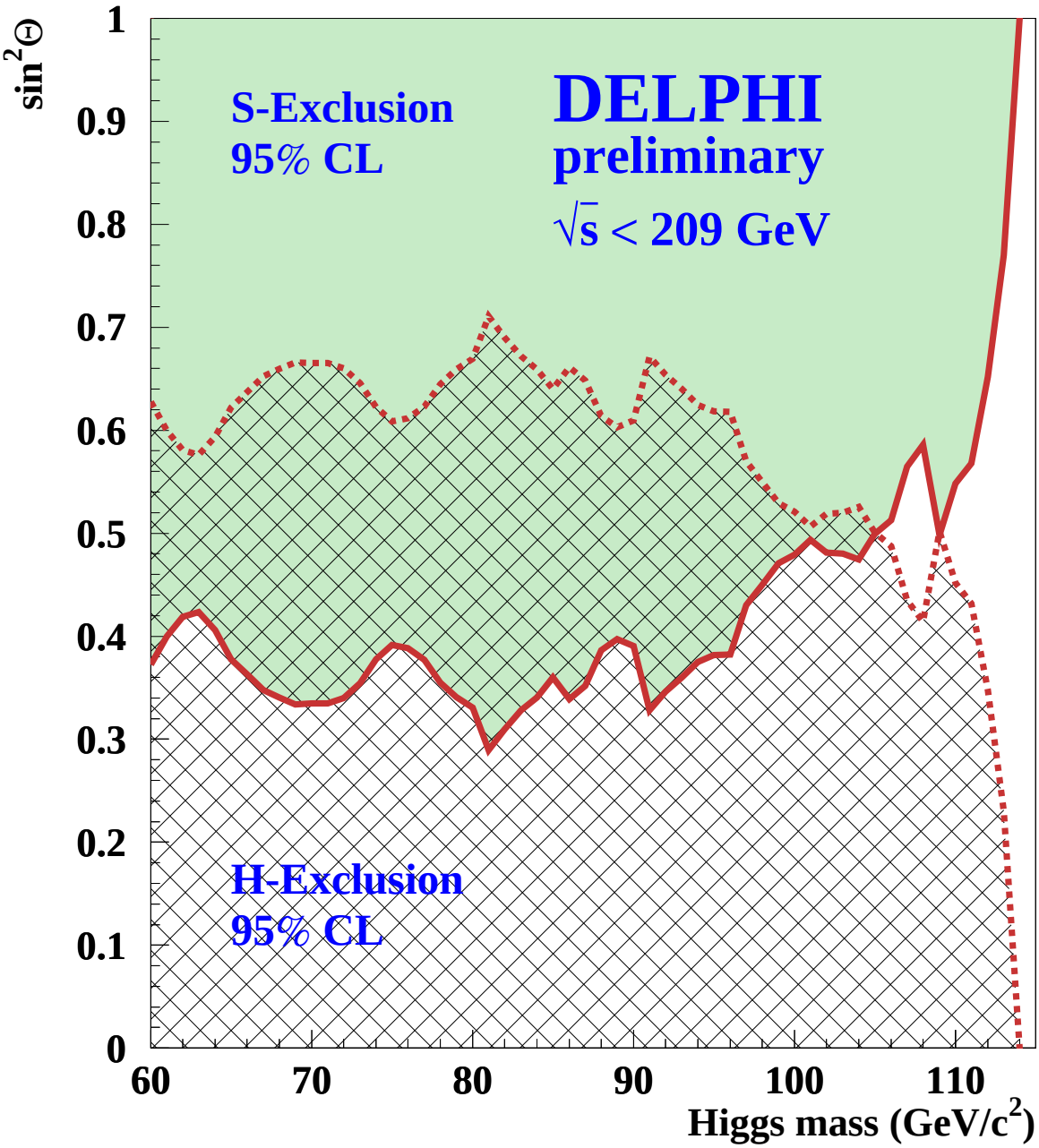

Figure 8: Limit on $\sin^2\theta$ as a function of the Higgs mass at 95% CL. S and H are the Higgs bosons in the Majoron model with expected production rates for large $\tan\beta$. In this case the Higgs boson only decays invisibly.